Aggregation and Disaggregation Kinetics of Human Blood Platelets: Part II. Shear-induced Platelet Aggregation

Pin Y. Huang* and J. David Hellums
Cox Laboratory for Biomedical Engineering, Rice University, Houston, Texas 77251-1892

ABSTRACT A population balance equation (PBE) mathematical model for analyzing platelet aggregation kinetics was developed in Part I (Huang, P. Y., and J. D. Hellums. 1993. *Biophys. J.* 65: 334-343) of a set of three papers. In this paper, Part II, platelet aggregation and related reactions are studied in the uniform, known shear stress field of a rotational viscometer, and interpreted by means of the model. Experimental determinations are made of the platelet-aggregate particle size distributions as they evolve in time under the aggregating influence of shear stress. The PBE model is shown to give good agreement with experimental determinations when either a reversible (aggregation and disaggregation) or an irreversible (no disaggregation) form of the model is used. This finding suggests that for the experimental conditions studied disaggregation processes are of only secondary importance. During shear-induced platelet aggregation, only a small fraction of platelet collisions result in the binding together of the involved platelets. The modified collision efficiency is approximately zero for shear rates below 3000 s^{-1}. It increases with shear rates above 3000 s^{-1} to about 0.01 for a shear rate of 8000 s^{-1}. Addition of platelet chemical agonists yields order of magnitude increases in collision efficiency. The collision efficiency for shear-induced platelet aggregation is about an order of magnitude less at 37°C than at 24°C. The PBE model gives a much more accurate representation of aggregation kinetics than an earlier model based on a monodispersed particle size distribution.

INTRODUCTION

Fluid mechanical shear stress can have profound effects on human blood cells. In particular, human blood platelets are very sensitive to shear stress as observed by morphological, biochemical, and functional changes. Several investigators have examined in vitro the effect of defined shear stresses on platelets (2–14). Shear stresses of 50 dynes/cm^2 and higher trigger platelet activation, cause the release of granule contents into the suspending medium, and elicit platelet aggregation. Higher shear stresses (100 dynes/cm^2) result in the appearance of nonstorage nucleotides and other cellular contents, indicating cell lysis. The response of platelets to agonists and plasma cofactors depends on the shear stress. Elevated shear stress is known to occur in arteries partially occluded by atherosclerosis or vasospasm as well as in artificial valves and circulation assistance devices. Thus, studies on kinetics and mechanisms of response to shear stress are of potential clinical value in understanding vascular disorders including thromboembolic events.

In Part I (1) a mathematical model incorporating both particle coalescence and breakage processes was developed to apply to platelet reactions under fluid mechanical shear stress. In this paper, this reversible population balance model is applied to match the evolution of observed particle volume density histograms by determination of the kinetic parameters of the model. These kinetic parameters, which include the collision efficiency for the aggregation processes and the breakage rate coefficient for the particle breakup processes, are used to provide insight into the activation of platelets and stability and cohesiveness of platelet aggregates.

Received for publication 25 June 1992 and in final form 11 February 1993.
Address reprint requests to J. D. Hellums.
* Now with Exxon Production Research, Houston, TX 77252-2189.

0006-3495/93/07/344/10 $2.00

EXPERIMENTAL METHODOLOGY

Platelet aggregation and disaggregation in the shear field were assessed by tracking changes in the particle size distribution. The experimental methodology is similar to that of Belval et al. (15). The procedure consists of four steps: preparation of a platelet suspension, aggregation by physical and chemical means, determination of the particle size distribution, and data reduction. The procedure is outlined below, and more details are given by Huang (16).

Platelet and viscometer preparation

Blood was obtained from healthy adults of age 20–50 by venipuncture into sterile disposable plastic syringes. The blood was then transferred into sterile siliconized glass tubes that contain sodium heparin (Elkins-Sinn Inc., Cherry Hill, NJ), 0.1 ml of anticoagulant solution (10 units/ml of whole blood)/10 ml of whole blood. The heparin-containing tubes were then capped and mixed by gentle inversion to inhibit further platelet activation and alkalosis. Centrifuging the blood at 150 *g* and 25°C for 15 min yielded a platelet-rich plasma (PRP) with a platelet count ranging from 240,000 to 500,000/μl. The remaining red cell plasma suspension was then centrifuged at 25°C for 15 min at 9,000 *g*, giving platelet-poor plasma (PPP). This PPP was used to dilute the PRP so that a platelet count of 280,000–350,000/μl was obtained.

A cone-plate viscometer (Ferranti-Shirley 781, Ferranti Electric Inc., England) applied the shear field to the platelet suspension. This viscometer consists of a stationary platen and a rotating cone (Fig. 1) that imposes a uniform shearing motion to the fluid medium. Throughout the shear experiments, a truncated cone with an angle of 1/3° is used. This cone gives a gap between the cone and platelet ranging from 30 μm at the center to 120 μm at the outside. The day before shear experiments, the cone and platen were treated to inhibit platelet-surface interaction by the following procedure. 1) Silicone solution consisting of 1 part Prosil-28 (PCR Research Chemicals; Gainesville, FL) and 100 parts of distilled water was loaded into the gap between the cone and platen and left for 1 h. 2) The cone and platen were then cleaned with deionized water and dried overnight at room temperature.

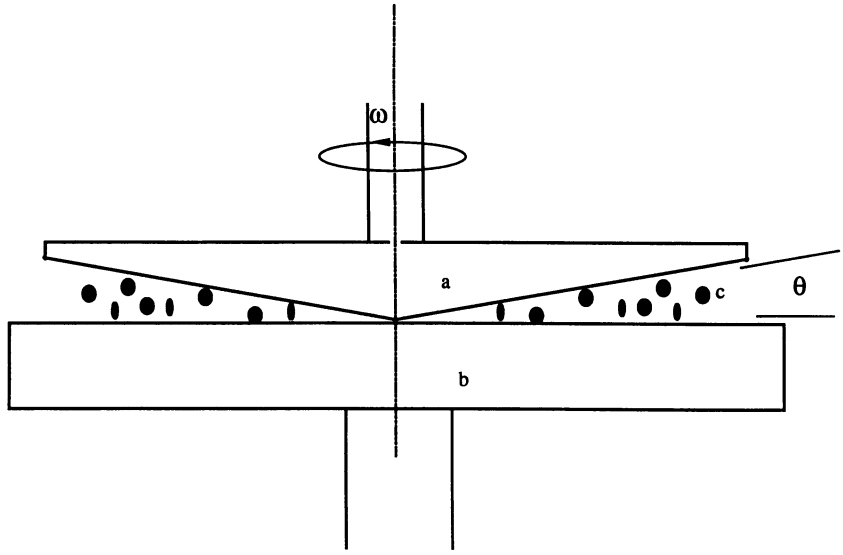

FIGURE 1 Cutaway schematic view of a cone-plate viscometer showing (*a*) rotating truncating cone (*b*) stationary plate (*c*) platelet suspension. A platelet suspension between the cone and the plate is subjected to a known, uniform shearing stress for a specified period of time. Subsequently a specimen is fixed and its particle size distribution determined electronically.

Specimens were subjected to a constant, uniform shear rate in the range of 3200 to 10,054 s^{-1}, for exposure times in the shear field ranging from 20 to 100 s. Shear studies were carried out at both 24 and 37°C. For experiments carried out at 37°C, platelet suspensions were incubated in a water bath at 37°C for 5 min before the application of shear force. Incubation time was set at 5 min, because storage of PRP at higher temperatures is known to age the platelets more rapidly (17, 18). The addition of any reagent during the shear experiment was accomplished by placing the tips of a precision Hamilton microsyringe in the shearing fluid and infusing the syringe content without stopping the shearing.

Particle size distributions

An electronic particle counter (Coulter Multisizer, Coulter Electronic, Hialeah, FL) was used to measure the particle size distribution of the samples. In the following discussion, particle volumes are expressed as the diameter of an equivalent rigid sphere. The particle counter is calibrated with rigid spheres, and it is known that flexible, nonspherical shapes give somewhat different response. Particles in the diameter range from 1.0 to 12.7 μm were measured by the use of a 50-μm diameter aperture, and particles in the diameter range from 6.4 to 168 μm were measured by the use of a 280-μm diameter aperture. The sedimentation velocity of the particles during counting was estimated by Bell et al. (13, 14) using the Stokes equation. For the largest particles counted by the use of the 50-μm aperture tube, they found sedimentation to be negligible. However, counting by the use of the 100-μm aperture tube, they observed that the largest particle sedimented 17 mm in 100 s. To avoid sedimentation problems, particles were kept in suspension during counting by constant stirring with a four-blade stirrer paddle (Coulter Electronics). For the 50-μm aperture, particles in 100 μl of electrolyte were counted. Because relatively few large aggregates are formed in the suspension, results with the large aperture tube tended to give a scattered histogram. Therefore, particles in 2000–4000 μl of electrolyte were counted to correct this problem. In all particle sizing, the coincidence correction (described in the Coulter Manual (19)) was kept below 3% of the raw count.

Several investigators, including Nichols and Bosmann (20) and Goldblum et al. (21), have studied the changes in the platelet size distributions and the degree of quenching of platelet reactions using various types and concentrations of fixatives. Results by these investigators show that there are artifacts associated with the fixation of cells due to changes in size and deformability. However, careful use of electronic particle size data can provide approximations of value in understanding platelet aggregation kinetics. Kinetic studies of platelet aggregation depend heavily on the ability to stop the processes before dilution, fixation, and electronic size distribution analysis (21, 22). Pilot studies (16) were carried out on the influence of glutaraldehyde concentration on platelet aggregates in the cone-plate viscometer using various glutaraldehyde concentrations both in the diluent and in the aggregated sample. Based on these studies, a final concentration of 0.05% w/v of glutaraldehyde was injected directly into the viscometer immediately prior to the cessation of shear stress exposure. Then the samples were diluted at least 1000-fold into Isoton II electrolyte (Coulter Electronics) containing 0.25% w/v glutaraldehyde concentration, and counted immediately on the 50-μm aperture. Particle sizing using the 280-μm aperture was usually completed within 6 h. A sample of the unsheared platelet suspension treated in the same way as sheared samples served to give the baseline particle size distribution.

Data reduction

A microcomputer interfaced with the electronic particle counter recorded the histograms. Three duplicate particle counts were performed for each sample, and the following computational processes were executed as follows. 1) Construct the size distribution from the number density data; 2) apply a moving average to smooth the raw data; 3) average multiple Coulter counter runs from the same sample; 4) splice the data from the 50- and 280-μm apertures; 5) convert number density from number of counts/channel to number density/dimensionless logarithmic scale; and 6) smooth the spliced data with a cubic spline.

Instrument calibration constants for 50- and 280-μm apertures were determined using 5.0- and 40-μm spherical latex particle calibration kits (Coulter Electronics). The instrument was also calibrated with a platelet standard control (American Dade, American Hospital Supply Corp. Miami, FL). The mean platelet volume, v_o, was calculated from the ratio of total volume to total population:

$$V_o = \frac{\int_{v_o}^{\infty} vn(v,t)\,dv}{\int_{v_o}^{\infty} n(v,t)\,dv} \quad (1)$$

These values were found to be 12 ± 2 (mean ± SE) μm^3 for the unaggregate suspensions. Thus, $x = 1$ in the results to be reported corresponds to this volume.

RESULTS

In this section, analyses are presented of shear-induced platelet aggregation kinetics by use of population balance mathematics. The model accounts for both aggregation and breakage due to splitting (the reversible model). Kinetic results are

also analyzed using the pure coalescence or irreversible model. In the irreversible model, two parameters (ϕ_a and ϵ) are varied; and in reversible model, three parameters (ϕ_a, ϵ, and k_1) are varied. The equations and definitions of the parameters are given in the preceding paper (1).

Experimental results

For the stress conditions used in this work, only a very small fraction of the platelets are lysed. The observed reductions in particle count are almost entirely due to aggregate formation. Typical results expressed as number and volume density distributions plots for shear-induced aggregation at various shear rates are given in Figs. 2 and 3. In these figures, the vertical lines represent the joint of two particle size distributions from both the 50- and 280-μm apertures. At time $t = 0$, shear stress is applied to the platelet-rich plasma (300,000 platelets/μl) to initiate aggregation. At the relatively low shear rate of 3600 s^{-1}, 60 s of exposure to shear results in a decrease in the total population, P, from 1.0 to 0.8, in a decrease of the singlet peak, and in the formation of small and intermediate size aggregates (Fig. 2). The formation of intermediate size aggregates is more apparent when the same information is replotted in volume density form (Fig. 3). In the volume density plot, the spread of the mass over various particle sizes is much more visible. At the higher shear rate of 5400 s^{-1}, platelets and small aggregates that exist at lower shear stress combined with each other to form larger aggregates as shown in the number density plot of Fig. 2. A distinctive bimodal distribution is obtained when the same information is constructed in volume density form (Fig. 3). At a still higher shear stress of 6300 s^{-1}, more large aggregates are formed as shown by the shifting of the mode of second peak to the right in the volume density curve.

Comparison of experimental and calculated size distributions

Comparisons are given between calculated distributions and experimental observations at an early stage of platelet aggregation in terms of the number density distribution (Fig. 4) and in terms of volume density distribution (Fig. 5). Here P is the total population of the particles expressed as a fraction of the initial, unaggregated population. Thus, $p = 0.82$ in Fig. 4 corresponds to a diminution of the initial particle count by 18%. The initial condition, corresponding to the unsheared PRP, is given by open squares. Experimental results, given by open circles, are for platelet-rich plasma subjected to a 20-s exposure at a shear rate of 5400 s^{-1}. Computed curves using both the pure coalescence model and the reversible model are given by open triangles and a curve, respectively.

At the onset of the shear aggregation, the total number of singlets in suspension was reduced as shown by the diminished singlet peak ($x \approx 1$) as compared to the initial distribution (Fig. 4). These singlets reappeared as aggregates as shown by the right shoulder on the singlet peak ($x > 4$). This decrease in singlets and formation of larger aggregates is captured by both the pure coalescence model and the reversible model. Both models give good agreement with the experimental observations. In volume density form (Fig. 5), more emphasis is placed on the larger aggregates in the suspension ($x > 4$). Once more, good agreement is obtained between the calculated and experimental results. The abrupt change in the calculated histogram at $x = 2$ is due to fact that a step function is used to describe $\phi(x)$. Two observations from these results are: 1) the value of ϵ is of the order of 10^{-3}, which means that, out of 1000 collisions, only one results in binding, and 2) the values of $\epsilon/(1 - \phi_a)$ for the reversible and irreversible models differ by only 4%.

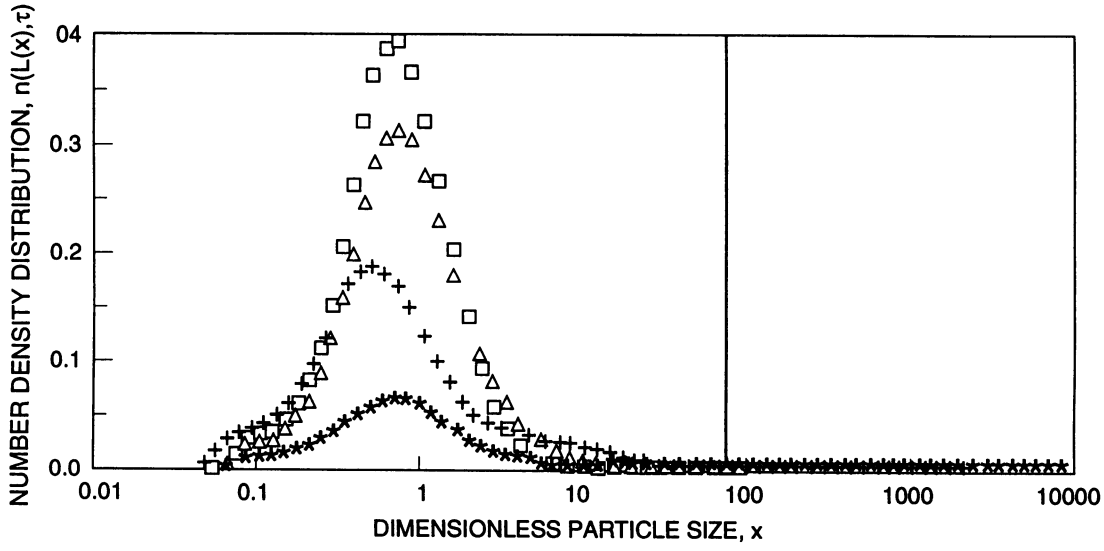

FIGURE 2 Spliced number density distributions for three different shear rates at a shear exposure time of 60 s at 24°C. (□) Histogram before exposure to the shear field; (△) histogram subjected to 3600 s^{-1} shear rate; (+) histogram subjected to 5400 s^{-1} shear rate; and (*) histogram subjected to 6300 s^{-1} shear rate. The vertical line denotes the particle volume category where results from the 50 and 280-μm aperture are spliced together.

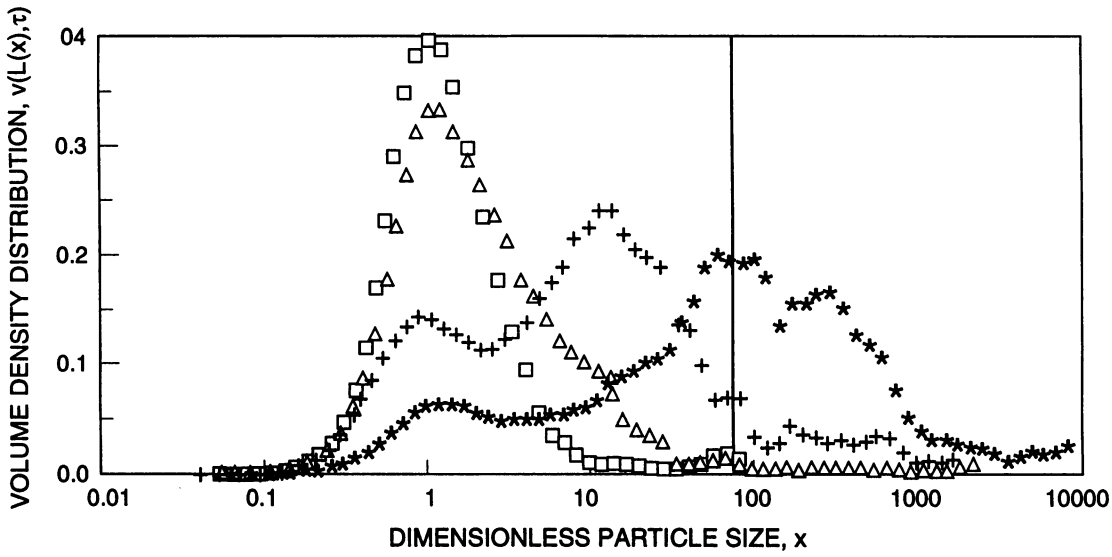

FIGURE 3 Spliced volume density distributions for three different shear rates at shear exposure time of 60 s at 24°C. (□) Histogram before exposure to the shear field; (△) histogram subjected to 3600 s^{-1} shear rate; (+) histogram subjected to 5400 s^{-1} shear rate; and (*) histogram subjected to 6300 s^{-1} shear rate. The vertical line denotes the particle volume category where results from the 50 and 280-μm aperture are spliced together. The distributions are for the same experimental results as in Fig. 2.

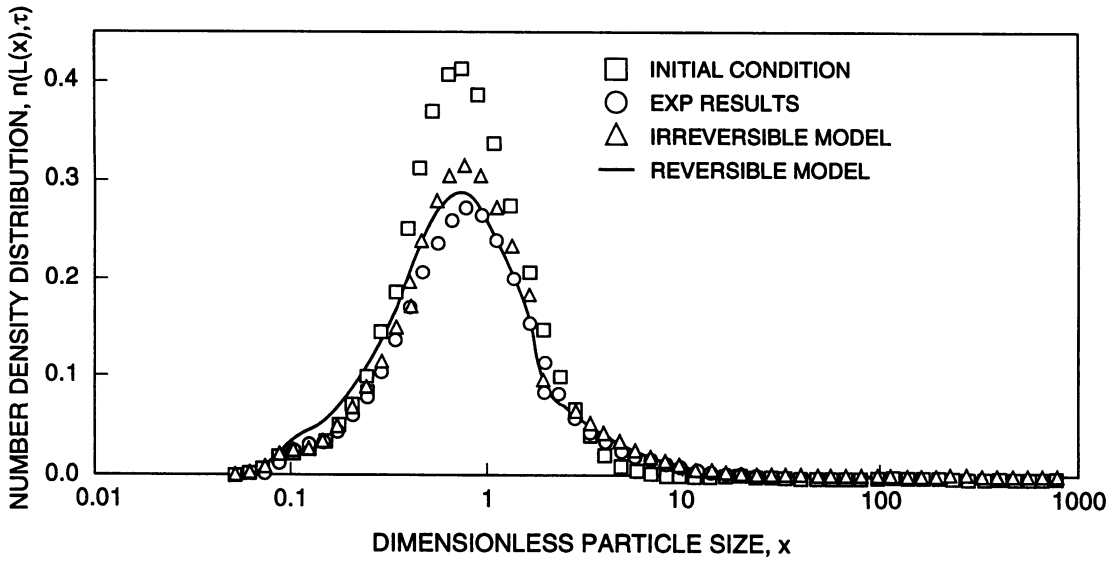

FIGURE 4 Comparison of observed and predicted number density histograms at an initial stage of shear-induced aggregation (p = 0.82): (□) Histogram before shear stress; (○) histogram for PRP following 20-s exposure to G = 5400 s^{-1} at 24°C; (△) pure coalescence solution with $\epsilon = 2.4 \times 10^{-4}$ and $\phi_a = 0.65$; and (–) reversible model solution with $\epsilon = 2.8 \times 10^{-4}$, $\phi_a = 0.61$ and $k_1 = 3.3 \times 10^{-4}$. All histograms other than the initial histogram have the same dimensionless volume and time.

Figs. 6 and 7 give comparisons between calculated and experimental results for an advanced (p = 0.2) stage of aggregation. In the more advanced stages of aggregation, the distribution takes on a distinctive bimodal shape as shown in the volume density plots. In all cases, good agreement is seen between the calculated and observed distributions. The differences between the experimental observation and the calculated results seem to be within the range of the experimental reproducibility. These deviations in reproducibility may include contributions related to the sampling and analytical methods (quenching of platelet reactions, sample dilution, particle sizing). Also, particle counts in the important large particle size range tend to be more scattered since fewer aggregates are detected in that range. As a result, scattering in the histogram is more pronounced when it is presented in volume density form.

The results in Figs. 2–7 were for shear-induced platelet aggregation at 23°C. Several studies of shear-induced platelet aggregation were carried out at 37°C. Figs. 8 and 9 give comparisons between the calculated and experimental results

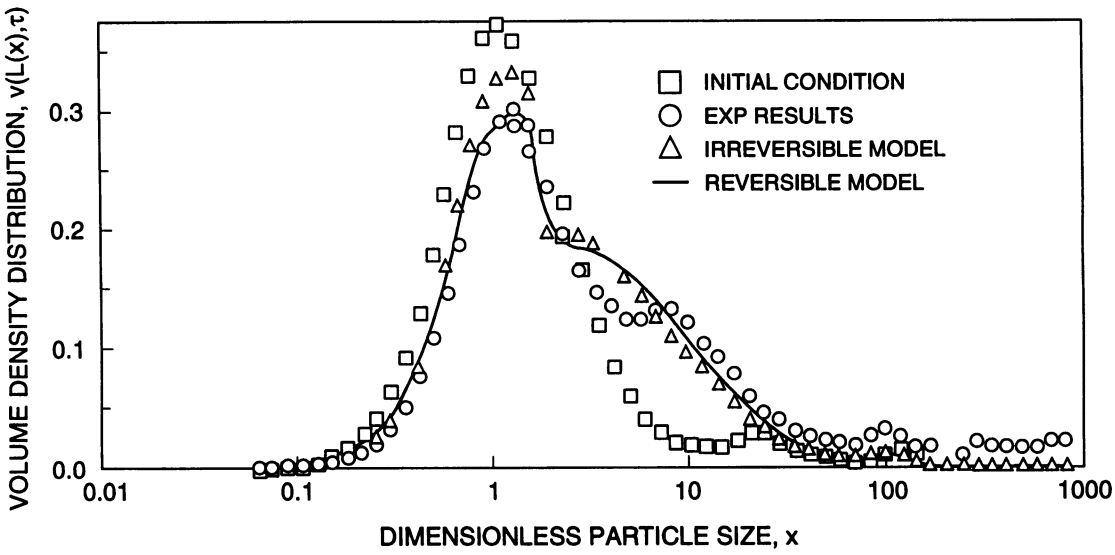

FIGURE 5 Comparison of observed and predicted volume density histograms at an initial stage of shear-induced aggregation (p = 0.82): (□) Histogram before shear stress; (○) histogram for PRP following 20-s exposure to $G = 5400\ s^{-1}$ at 24°C; (△) pure coalescence solution with $\epsilon = 2.4 \times 10^{-4}$ and $\phi_a = 0.65$; and (–) reversible model solution with $\epsilon = 2.8 \times 10^{-4}$, $\phi_a = 0.61$ and $k_1 = 3.3 \times 10^{-4}$. All histograms other than the initial histogram have the same dimensionless volume and time.

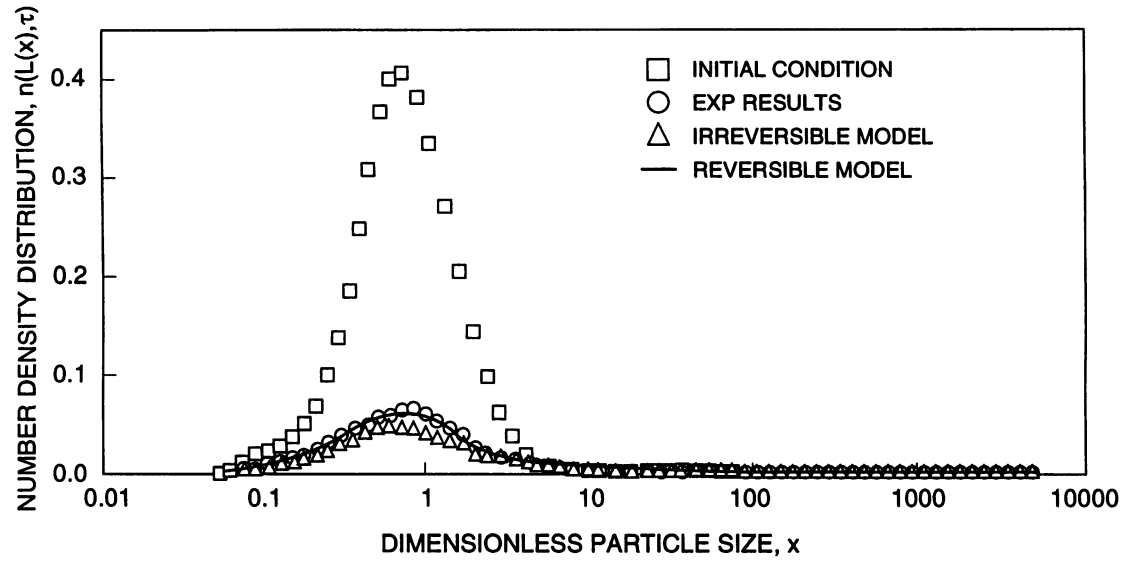

FIGURE 6 Comparison of observed and predicted number density histograms at an advanced stage of shear-induced aggregation (p = 0.20): (□) Histogram before shear stress; (○) histogram for PRP following 60-s exposure to $G = 6300\ s^{-1}$ at 24°C; (△) pure coalescence solution with $\epsilon = 1.6 \times 10^{-3}$ and $\phi_a = 0.4$; and (–) reversible model solution with $\epsilon = 1.2 \times 10^{-3}$, $\phi_a = 0.6$ and $k_1 = 1.2 \times 10^{-4}$. All histograms other than the initial histograms have the same dimensionless volume and time.

at a shear rate of $10{,}080\ s^{-1}$ and an exposure time of 60 s. The extent of platelet aggregation tends to be less at 37°C than at 23°C. Therefore, a higher shear rate and longer exposure time are used for a given degree of aggregation. The value of $\epsilon/(1 - \phi_a)$ is of the order of 10^{-4}—about an order of magnitude lower than the value at 23°C for the same conditions. The lesser aggregation could be related to the higher activity of ADPase enzymes at 37°C, and this is consistent with the reports by Cronberg (17) and Breddin and Krzywarek (18) that storing of PRP at 37°C rapidly aged the platelets.

Population balance parameters

The dependence of ϕ_a, ϵ, and k_1 on shear rates and shear history was examined. Shear-induced platelet aggregation was carried out at various shear rates ranging from $3600\ s^{-1}$ to $7650\ s^{-1}$ at exposure times of 40 and 60 s. Shear histories from 20 to 100 s were carried out at shear rates of $5400\ s^{-1}$ and $6300\ s^{-1}$. The ratio, $\epsilon/(1 - \phi_a)$, rather than the individual values of ϵ and ϕ, is reported for these studies, since, as explained in Part I (1), this ratio is a better correlator of results than either individual parameter.

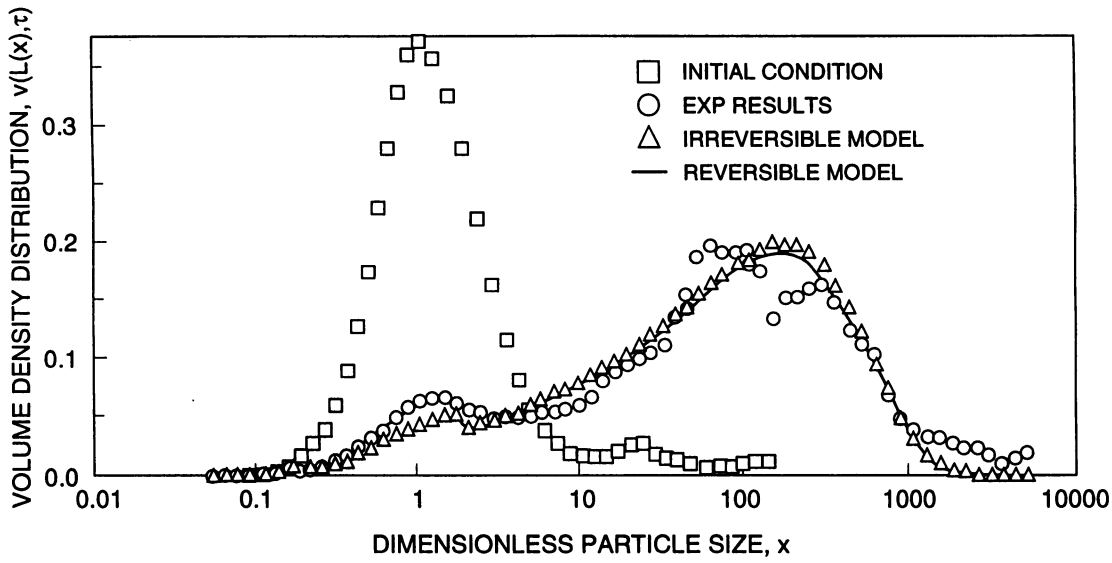

FIGURE 7 Comparison of observed and predicted volume density histograms at an advanced stage of shear-induced aggregation (p = 0.20): (□) Histogram before shear stress; (○) histogram for PRP following 60-s exposure to $G = 6300\ s^{-1}$ at 24°C; (△) pure coalescence solution with $\epsilon = 1.6 \times 10^{-3}$ and $\phi_a = 0.4$; and (–) reversible model solution with $\epsilon = 1.2 \times 10^{-4}$, $\phi_a = 0.6$ and $k_1 = 1.2 \times 10^{-4}$. All histograms other than the initial histograms have the same dimensionless volume and time.

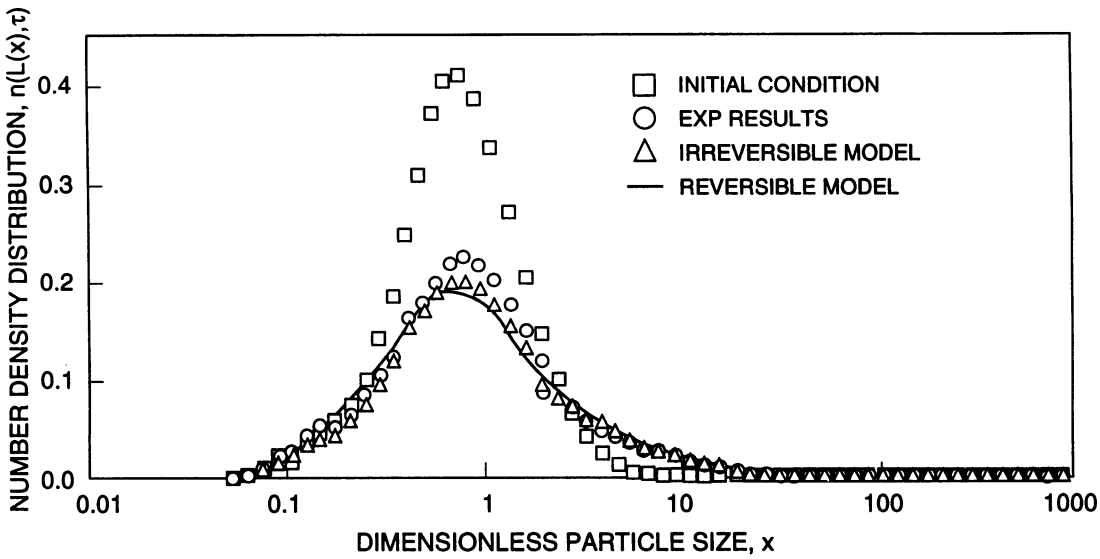

FIGURE 8 Comparison of observed and predicted number density histograms at an initial stage of shear-induced aggregation (p = 0.70) at 37°C: (□) Histogram before shear stress; (○) histogram for PRP following 60-s exposure to $G = 10800\ s^{-1}$; (△) pure coalescence solution with $\epsilon = 2.0 \times 10^{-4}$ and $\phi_a = 0.6$; and (–) reversible model solution with $\epsilon = 2.4 \times 10^{-4}$, $\phi_a = 0.55$ and $k_1 = 1.7 \times 10^{-4}$. All histograms other than the initial histograms have the same dimensionless volume and time.

In Fig. 10, it can be seen that collision efficiency increases moderately with exposure time to shear stress over the range of 20 to 100 s. Similarly, it can be seen in Fig. 11 that collision efficiency is a slowly increasing function of shear rate over the range of 3600 to 5400 s^{-1}, but increases more rapidly with higher shear rates. These findings are consistent with the results reported by Belval and Hellums (7), but Belval and Hellums showed that for smaller exposure times (10 s) the collision efficiency is higher than at 20 s. They also found evidence that at very high shear rates (10,000 s^{-1} the collision efficiency decreases.

The breakage rate constant, k_1, was found to be independent of both shear rate and time history (not shown). The breakage rate constant, k_1, was found to be at a low, nearly constant level of about 3.0×10^{-4}. This finding is consistent with the comparison studies of calculated and experimentally observed particle size distributions (Figs. 4–7). As shown in those figures, the reversible and irreversible models give al-

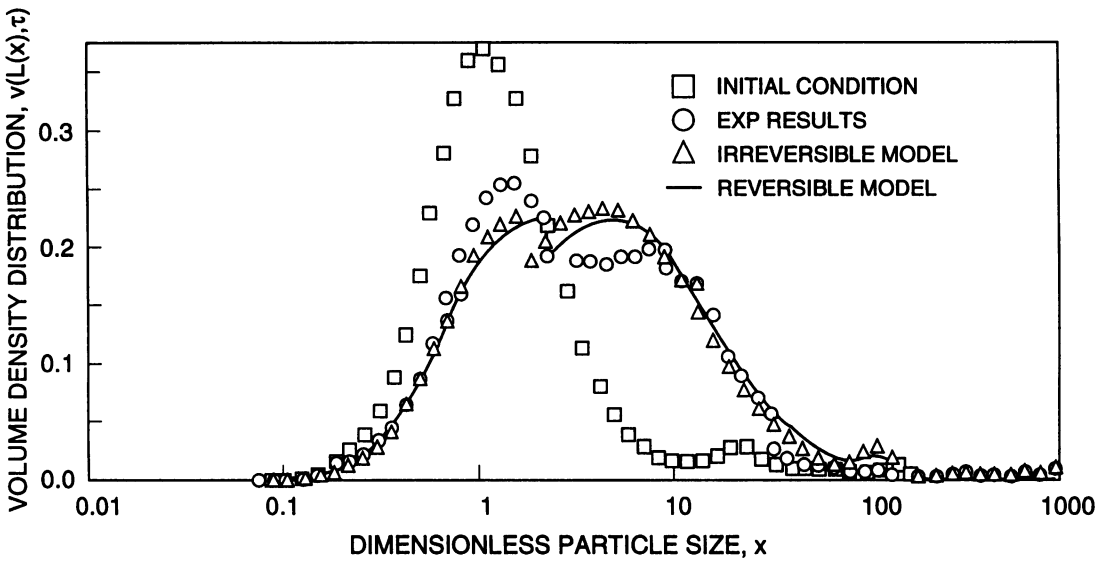

FIGURE 9 Comparison of observed and predicted volume density histograms at an initial stage of shear-induced aggregation (p = 0.70) at 37°C: (□) Histogram before shear stress; (○) histogram for PRP following 60-s exposure to $G = 10800\ s^{-1}$; (△) pure coalescence solution with $\epsilon = 2.0 \times 10^{-4}$ and $\phi_a = 0.6$; and (–) reversible model solution with $\epsilon = 2.4 \times 10^{-4}$, $\phi_a = 0.55$ and $k_1 = 1.7 \times 10^{-4}$. All histograms other than the initial histograms have the same dimensionless volume and time.

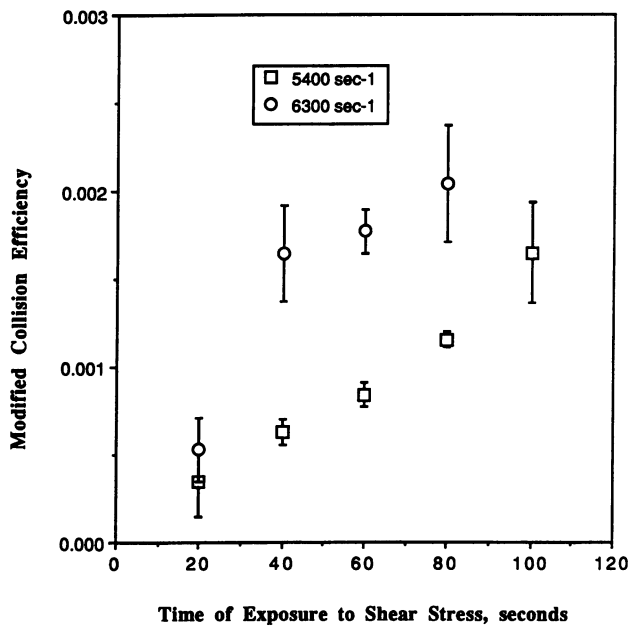

FIGURE 10 The dependence of the modified collision efficiency, $\epsilon/(1 - \phi_a)$, on exposure time to the shear field for shear rates of 5400 and 6300 s^{-1} at 24°C. Each data point represents the mean ± SE for four to five experiments from the same donor.

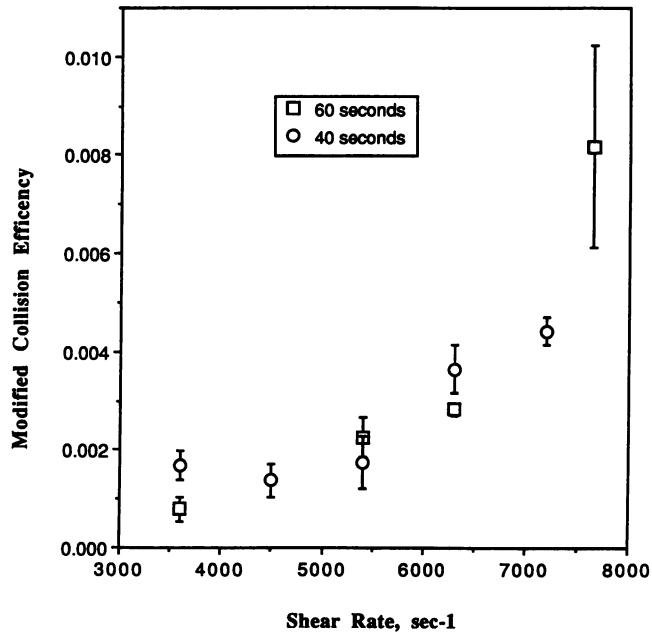

FIGURE 11 The dependence of the modified collision efficiency, $\epsilon/(1 - \phi_a)$, on exposure time to the shear field for shear rates of 5400 and 6300 s^{-1} at 24°C. Each data point represents the mean ± SE for four to five experiments form the same donor.

most identical calculated histograms. The estimates of modified collision efficiency from the two models differ only by 4–16%. The values of the objective function obtained using the pure coalescence or the reversible model differ by no more than 1.4×10^{-2}. These results suggest that the breakage events are not important under the experimental conditions studied. Confirmation of this finding was obtained by solution using $k_1 = 0$ (the irreversible model). These solutions yielded essentially the same calculated histogram as the more complete model including disaggregation.

Comparison with prior, simpler models

Estimates of the modified collision efficiency were compared with results obtained using simpler models. Assuming no aggregate breakup or formation of high order aggregates

in the suspension, Bell et al. (13, 14) modeled platelet aggregation using first order kinetics with respect to total dimensionless population P. The equation used in their analysis is given by (Swift and Friedlander (23)),

$$dP/dt = -4\bar{G}\epsilon\Lambda P/\pi \quad (2)$$

with $P(0) = 1$, the initial population. Integration of the Eq. 2 yields:

$$\ln(P) = -4\bar{G}\epsilon\Lambda t/\pi \quad (3)$$

where ϵ is the collision efficiency, $\bar{G}$ is mean shear rate, and Λ is the volume fraction of the platelets in the suspension. Estimates for ϵ were calculated using Eq. 3 applied to the experimental population data of this work. These values of ϵ were then compared to values of $\epsilon/(1 - \phi)$ determined by application of the model of this work to the same data. The results, expressed as a percent difference in ϵ, are given in Fig. 12 as a function of the final total population. For the initial stage ($p > 0.9$) of shear aggregation, the simple method gives relatively good agreement. However, for intermediate and advanced stages of aggregation ($p < 0.9$), the values for ϵ calculated using the simple model deviate from the estimates for $\epsilon/(1 - \phi)$ calculated using the model of this work. The difference lies in the assumption of Eq. 3 that the suspension is not polydispersed. Equation 3 treats each particle the same—independent of particle volume. It can be shown that the model of this work is equivalent to Eq. 3 for the initial instant of application to a monodispersed initial distribution.

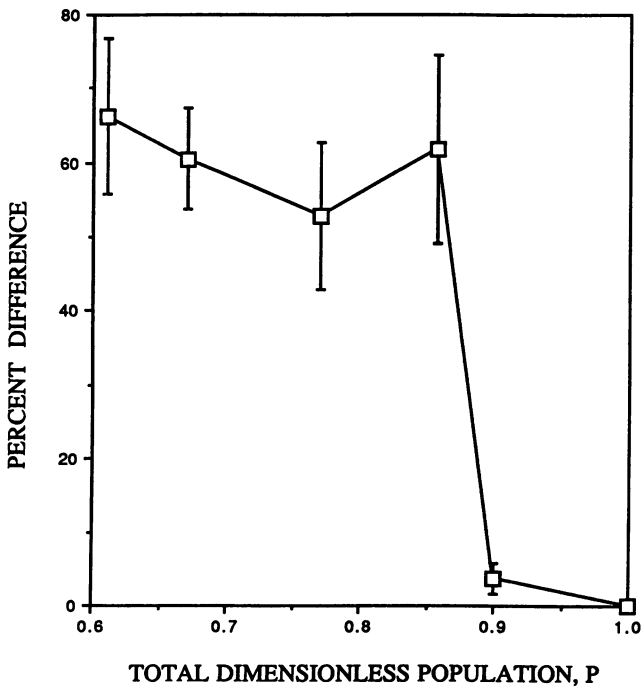

FIGURE 12 Differences in the estimates for $\epsilon/(1 - \phi_a)$ with that of ϵ_o using the simplified model by Swift and Friedlander (1964). Each data point represents the mean ± SE of four experiments from the same donor.

Using the discrete form of the Smoluchowski's equation, Chang and Robertson (24) reported collision efficiencies of 0.1–0.2 for the ADP-induced aggregation (0.5–100 μM ADP) of rabbit platelets at low shear rates (20–80 s^{-1}). In the present work, at a shear rate of 450 s^{-1} and at a final ADP concentration of 0.25 μM, the estimate for the modified collision efficiency is about 0.06 at $T = 37°C$. These findings illustrate the extreme sensitivity of the collision efficiency to activation of platelets by agonists: values of the collision efficiency range from 10^{-4} and less for shear-induced aggregation, to 0.06 for the low dosage of ADP, to 0.2 for a moderate dosage of ADP.

DISCUSSION

The principal findings in this study of shear stress-induced platelet aggregation are reviewed below.

1) Good agreement is obtained between experimental observations and model predictions using either the irreversible coalescence model or the reversible model. The two models give collision efficiencies different by only 6–16% for shear-induced aggregation.

2) During shear-induced platelet aggregation, only a small fraction of platelet collisions result in the binding together of the involved platelets. The modified collision efficiency is approximately zero for shear rates below 3000 s^{-1}. It increases with shear rates above 3000 s^{-1} to about 0.01 for a shear rate of 8000 s^{-1}. In that case about one collision in a hundred results in binding. Added chemical platelet agonists can increase the collision efficiency by one or more orders of magnitude.

3) Under the test conditions, the breakage rate constant is observed to be independent of the shear rate, and the breakage processes are of only secondary importance. The lack of dependence of the breakage rate constant on the shear rate suggests a competition between two opposing influences: increasing platelet activation versus increasing shear forces acting to destroy platelet aggregates.

4) The collision efficiency for shear-induced platelet aggregation is about an order of magnitude less at 37°C than at 23°C.

5) Simple analytical models of aggregation based on a monodispersed particle size distribution can accurately represent the early stages of aggregation. However, these models are in significant error for extents of aggregation greater than about 15%.

As suggested by Belval and Hellums (7), an advantage of using the PBE to model the platelet reaction kinetics is that the parameters in the model are closely related to physical characteristics of platelets and platelet aggregates. For example, the estimated collision efficiency reflects binding affinity of particles for one another. Platelets develop this binding affinity as a result of activation by physical or chemical stimuli. Thus the estimate of the collision efficiency can be used to characterize the state of platelet activation. Similarly, the breakage rate constant reflects the stability of platelet aggregates in the shear field.

The increase in the modified collision efficiencies with respect to shear rate and time are consistent with the notion of different types of binding at low and high shear rates as reported by Bell et al. (13, 14) for aggregation in the presence of added ADP. At high shear rates and long exposure times, after a brief delay, a relatively shear-resistant bond appears to be formed.

These results are consistent with the findings of Belval and Hellums (7) and Moake et al. (25) that suggest the shear-induced platelet aggregation is mediated by ADP released from the dense granules. Platelets tend to follow the fluid stream lines and rotate with a frequency proportional to the fluid shear rate. Platelets experience a time-dependent surface shear stress and will deform due to the flexibility of the membrane. If the shear stress exceeds a threshold level, it is known that intracellular ADP will appear in the extracellular fluid. At higher shear stress, the quantity of liberated ADP increases, consistent with the increase in the modified collision efficiency with increasing shear rates and times. However, there is some disagreement among the prior workers on whether the shear stress directly stimulates the platelet-release reaction, or whether the initial extracellular ADP is a result of lysis-leakage related to membrane fatigue (2, 5, 6, 8, 26, 27). In Voisin's studies (8), plasma lactate dehydrogenase activity, an indicator of shear-induced platelet lysis, was observed to increase only at shear rates above 7000 s^{-1}, while β-thromboglobulin release (an indicator of platelet-release reaction) occurred at shear rates of 3000 s^{-1}. Additional evidence supporting the shear-induced platelet activation mechanism comes from studies on the roles of platelet membrane receptors and plasma proteins (25, 28). For shear-induced platelet aggregation to occur, platelet membrane glycoprotein receptors GPIb and GPIIb/IIIa are required, along with extracellular calcium ion and von Willebrand factor (vWf). GPIb and vWF are not required for aggregation in response to ADP at the low stress levels employed in aggregometry.

In this paper the population balance model was applied to the analysis of experimental results under circumstances where it was found that coalescence (aggregation) processes were of dominant importance, and reversibility (disaggregation) was of only secondary importance. In the third paper of this sequence (29), the model is applied to analysis of experiments wherein reversibility (disaggregation) is known to be important: disaggregation of platelet aggregates formed in response to the addition of low dosage ADP.

GLOSSARY

Nomenclature

$\bar{G}$ mean shear rate, s^{-1}

P total dimensionless particle population expressed as a fraction of the initial platelet population.

t time (in seconds)

Greek symbols

ϵ collision efficiency

τ' shear stress (dynes/cm^2)

Λ volume fraction of platelets in suspension, dimensionless

ϕ_a void fraction related to collision diameter, dimensionless

This work was supported by the National Institutes of Health under Grants 5P50NS23327 and 5R3718584.

REFERENCES

1. Huang, P. Y., and J. D. Hellums. 1992. Aggregation and disaggregation kinetics of human blood platelets: part I. Development and validation of a population balance method. *Biophys. J.* 65:334-343.
2. Brown, C. H., L. B. Leverett, C. W. Lewis, C. P. Alfrey, and J. D. Hellums. 1975. Morphological biochemical and functional changes in human platelets subjected to shear stress. *J. Lab. Clin. Med.* 86:462–471.
3. Klose, J. H., H. Reiger, and H. Schmid-Schonbein. 1975. A rheological method for the quantification of platelet aggregation in-vitro and its kinetics under flow conditions. *Thromb. Res.* 22:445–455.
4. Yung, W., and M. M. Frojmovic. 1982. Platelet aggregation in laminar flow. Part I: Adenosine diphosphate concentration, time, and shear rate dependence. *Thromb. Res.* 28:361–378.
5. Anderson, G. H., J. D. Hellums, J. Moake, and C. P. Alfrey. 1978. Platelet lysis and aggregation in shear fields. *Blood Cells* 4:499–507.
6. Anderson, G. H., J. D. Hellums, J. Moake, and C. P. Alfrey. 1978. Platelet response to shear stress: change in serotonin uptake, serotonin release, and ADP-induced aggregation. *Thromb. Res.* 27:316–330.
7. Belval, T. K., and J. D. Hellums. 1986. Analysis of shear-induced platelet aggregation with population balance mathematics. *Biophys. J.* 50: 479–487.
8. Voisin, P., C. Guimont, and J. F. Stoltz. 1985. Experimental investigation of the rheological activation of blood platelets. *Biorheology.* 22:425–435.
9. Dewitz, T. S., R. R. Martin, R. T. Solis, J. D. Hellums, and L. V. McIntire. 1978. Microaggregate formation in whole blood exposed to shear stress. *Microvasc. Res.* 16:263–271.
10. Jen, C. J., and L. V. McIntire. 1984. Characteristics of shear-induced aggregation in whole blood. *J. Lab. Clin. Med.* 103:115–124
11. Alkhamis, T. M., R. L. Beissinger, and J. Chedian. 1987. Effect of red blood cells on platelet adhesion and aggregation in low-stress shear flow. *Trans. Am. Soc. Artif. Intern Organs.* 33:636–642.
12. Alkhamis, T. M., R. L. Beissinger, and J. Chedian. 1990. Artificial surface effect on red blood cells and platelets in laminar shear flow. *Blood.* 75:1568–1575.
13. Bell, D. N., S. Spain, and H. L. Goldsmith. 1989. The ADP-induced aggregation of human platelet in flow through tubes. II. Effect of shear rate, donor sex and ADP concentration. *Biophys. J.* 56:829–843.
14. Bell, D. N., S. Spain, and H. L. Goldsmith. 1989. The ADP-induced aggregation of human platelet in flow through tubes. I. Measurement of the concentration and size of single platelets and aggregates. *Biophys. J.* 56:817–828.
15. Belval, T. K., J. D. Hellums, and R. T. Solis. 1984. The kinetics of platelet aggregation induced by fluid shearing stress. *Microvasc. Res.* 28:279–288.
16. Huang, P. Y. 1991. The kinetics of human platelet aggregation and disaggregation in controlled shear field. Ph.D. thesis. Rice University, Houston, TX. 1–233.
17. Cronberg, S. 1970. Evaluation of platelet aggregation. *Coagulation.* 3:139–151.
18. Breddin, K., and H. J. Krzywarek. 1977. Platelet aggregation. *Thromb. Haemost.* 38:252–259.
19. Coulter. 1987. Reference Manual for Coulter Multisizer: Fine Particle Application Notes. Coulter Electronic, Hialeah Florida. 2–5 to 2–9.
20. Nichols, A. R., and H. B. Bosmann. 1979. Platelet aggregation: newly quantified using nonempirical parameters. *Thromb. Haemost.* 42:679–693.
21. Goldblum, D. K., J. K. Horak, J. D. Hellums, and R. T. Solis. 1985. Stabilization of platelet aggregate size distributions by glutaraldehyde. *Thromb. Res.* 40:249–255.

22. Wurzinger, L. J., R. Opitz, and H. Schmid-Schonbein. 1988. Effect of anticoagulants on shear-induced platelet aggregations. *Thromb. Res.* 49:133–137.
23. Swift, D. L., and S. K. Friedlander. 1964. The coagulation of hydrosol by Brownian motion and laminar shear flow. *J. Colloid Sci.* 19:621–647.
24. Chang, H. N., and C. R. Robertson. 1976. Platelet aggregation by laminar shear flow and Brownian motion. *Ann. Biomed. Eng.* 4:151–183.
25. Moake, J., N. A. Turner, L. Nolasco, and J. D. Hellums. 1988. Shear-induced platelet aggregation can be mediated by vWf release from platelet, as well as exogenous large or or unusually large vWf multimers, requires adenosine diphosphate, and is resistant to aspirin. *Blood.* 71:1366–1374.
26. Wurzinger, L. J., R. Opitz, P. Balsberg, and H. Schmid-Schonbein. 1985. Platelet and coagulation parameters following millisecond exposure to laminar shear stress. *Thromb. Haemost.* 54:381–386.
27. Wurzinger, L. J., R. Opitz, M. Wolf, and H. Schmid-Schonbein. 1985. Shear-induced platelet activation—a critical reappraisal. *Biorheology.* 22:399–405.
28. Peterson, D. M., N. A. Stathopulous, T. D. Giorgio, J. D. Hellums, and J. Moake. 1987. Shear-induced platelet aggregation requires von Willebrand factor and platelet glycoprotein Ib and IIb-IIIa. *Blood.* 69:625–628.
29. Huang, P. Y., and J. D. Hellums. 1992. Aggregation and disaggregation kinetics of human blood platelets: Part III. ADP-induced reversible Aggregation. *Biophys. J.* 65:354-362.